Tuning the Ferrotoroidic Coupling and Magnetic Hysteresis in Double-Triangle Complexes {Dy₃MᴵᴵᴵDy₃} via the Mᴵᴵᴵ-linker

Jared M. Ashtree,[a] Ivana Borilović,[b] Kuduva R. Vignesh,[c] Abinash Swain,[c] Sarah H. Hamilton,[d] Yasmin L. Whyatt,[d] Sophie L. Benjamin,[e] Wasinee Phonsri,[b] Craig M. Forsyth,[b] Wolfgang Wernsdorfer,[f] Alessandro Soncini,*[a] Gopalan Rajaraman,*[c] Stuart K. Langley,*[d] and Keith S. Murray*[b]

We present the syntheses, structures, magnetic data and theoretical analyses for two families of heptanuclear clusters, wherein two staggered dysprosium(III) triangles are linked by various M(III) d-/p-block ions. The families differ in the counter-anion and are of formulae [Dyᴵᴵᴵ₆Mᴵᴵᴵ(OH)₈(o-tol)₁₂(MeOH)₅(NO₃)]·4MeOH and [Dyᴵᴵᴵ₆Mᴵᴵᴵ(OH)₈(o-tol)₁₂(MeOH)₆]Cl·6MeOH (M = Cr, Mn, Fe, Co, Al; o-tol = o-toluate). We find that variation of the central metal ion M is crucial in tuning the toroidal moments on the triangular units, with diamagnetic M linking ions enhancing the ferrotoroidic coupling. By detailed simulation and analysis of various magnetic measurements, including sub-kelvin microSquid hysteresis loops, we identified the specific signature of the M linking ions' modulation of toroidal properties, including the mechanism whereby aniso-tropic, paramagnetic M ions lead to hysteresis profiles with larger remnant magnetisations and broader coercive fields.

Introduction

Lanthanide-containing molecular complexes have been inves-tigated over the last two decades for potential applications in quantum information processing,[1] high-density data storage, and nanoscale devices including molecular spin valves and transistors.[1a,2] By varying the coordination environments of lanthanide ions to influence their electronic structures, re-searchers seek to optimise molecule-based devices. For exam-ple, data storage devices benefit from longer relaxation times in single-molecule magnets (SMMs) whose moments have been manipulated by external fields.[3]

Of particular interest are single-molecule toroics (SMTs) with toroidal/vortex arrangements of spins,[4–6] which make SMTs less sensitive than SMMs to intermolecular interactions and homo-geneous magnetic fields, and thereby allow even closer packing of nanoscale devices.[5a] Also considering the potential to control the populations of toroidal states using charge/spin currents,[7–9] it is clear why research into SMTs is a priority area.

The first detailed examples of molecular toroidal moments were pioneering experimental[4] and theoretical[5] studies on strongly anisotropic spin rings in general,[5a] and a {Dy₃} triangular complex in particular.[4,5b] Further examples include other {Dy₃} triangles,[10] {Dy₄} squares[11] and cubanes,[12] and {Dy₆} hexagons[13] (see Figure S1 in SI). Toroidal moments in {Fe₈Dy₈} and {Cu₆Tb₆} rings can stem from Feᴵᴵᴵ–Dyᴵᴵᴵ/Cuᴵᴵ–Tbᴵᴵᴵ ferromagnetic exchange coupling,[14] and counter-rotating tor-oidal moments (antiferrotoroidic, AFT) were found in the ground state of a {Dy₈} molecule.[15] For the latest reviews of SMTs and ferrotoroidic materials, see Refs. 16 and 17, respectively.

Recently, we linked[18] two staggered {Dy₃} units with a six-coordinate Crᴵᴵᴵ in [CrᴵᴵᴵDyᴵᴵᴵ₆(OH)₈(o-tol)₁₂(NO₃)(MeOH)₅]·3MeOH (1; o-tol = o-toluate), where intra-triangle dipolar coupling produced separate toroidal moments on each {Dy₃} unit, and inter-triangle dipolar coupling led to a con-rotating, ferrotor-oidic (FT) ground state. Importantly, direct simulation of the spin dynamics of 1 revealed how the signature of low-energy FT states could be discerned from hysteresis measurements.[18]

It is clearly desirable to favourably tune the properties of 1 by systematically changing the Lnᴵᴵᴵ ion, central Mᴵᴵᴵ ion, solvent, carboxylate and co-anion. Initial work to replace Dy with Tb and Ho led to the first observation of ferrotoroidicity in these f-block

[a] J. M. Ashtree, Prof. A. Soncini
School of Chemistry, University of Melbourne,
Parkville, VIC 3010, Australia
E-mail: asoncini@unimelb.edu.au
www.sonciniresearchgroup.com
[b] Dr. I. Borilović, Dr. W. Phonsri, Dr. C. M. Forsyth, Prof. K. S. Murray
School of Chemistry, Monash University, Building 23,
17 Rainforest Walk, Clayton, VIC3800, Australia
E-mail: keith.murray@monash.edu
[c] Dr. K. R. Vignesh, A. Swain, Prof. G. Rajaraman
Department of Chemistry,
Indian Institute of Technology Bombay,
Powai, Mumbai, Maharashtra, 400 076, India
E-mail: rajaraman@chem.iitb.ac.in
https://ether.chem.iitb.ac.in/~rajaraman/
[d] S. H. Hamilton, Y. L. Whyatt, Dr. S. K. Langley
School of Science and the Environment,
Division of Chemistry
Manchester Metropolitan University,
Manchester, UK
E-mail: s.langley@mmu.ac.uk
[e] Dr. S. L. Benjamin
School of Science and Technology
Nottingham Trent University,
Nottingham NG11 8NS, UK
[f] Prof. W. Wernsdorfer
Institute of Quantum Materials and Technologies,
Karlsruhe Institute of Technology,
76344 Eggenstein-Leopoldshafen, Germany

EurJIC
European Journal of Inorganic Chemistry

Full Papers
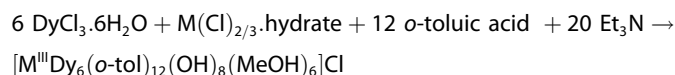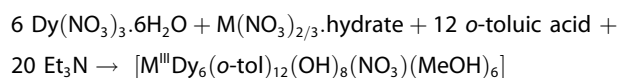**doi.org/10.1002/ejic.202001082**

Chemistry Europe
European Chemical Societies Publishing

ions.[19] Herein we discuss the effects of changing the M ions and counter-anions in the families [$M^{III}Dy^{III}_6(OH)_8$(o-tol)$_{12}$(NO$_3$)(MeOH)$_5$]·3MeOH (M = Mn-**2**, Fe-**3**, Co-**4**, Al-**5**) and [$M^{III}Dy^{III}_6$(OH)$_8$(o-tol)$_{12}$(MeOH)$_6$]Cl (M = Cr-**1'**, Mn-**2'**, Fe-**3'**, Co-**4'** Al-**5'**). We also determined the Mn anisotropy in **2'** by making [$Mn^{III}Y^{III}_6$(OH)$_8$(o-tol)$_{12}$(MeOH)$_6$]Cl (**6'**) with diamagnetic Y^{III}.

By combining experimental data with *ab initio* calculations and parameter-free models, we identified several trends in these complexes' structural, energetic and magnetic properties. In particular, we successfully implemented a strategy[18] to enhance the FT coupling, and proved that coupling between the toroidal states and the central ion is crucial to tune these systems' spin dynamics properties, specifically, to modulate their magnetic relaxation rates.

Results and Discussion

Synthesis

The nitrate and chloride families were prepared according to the following equations (details in SI):

6 Dy(NO$_3$)$_3$.6H$_2$O + M(NO$_3$)$_{2/3}$.hydrate + 12 o-toluic acid +

20 Et$_3$N → [M^{III}Dy$_6$(o-tol)$_{12}$(OH)$_8$(NO$_3$)(MeOH)$_6$]

6 DyCl$_3$.6H$_2$O + M(Cl)$_{2/3}$.hydrate + 12 o-toluic acid + 20 Et$_3$N →

[M^{III}Dy$_6$(o-tol)$_{12}$(OH)$_8$(MeOH)$_6$]Cl

Crystal structures show subtle changes between families

In both families, two staggered {Dy$_3$} triangles lie above and below a trivalent d-/p-block ion (Figure 1). The nitrates **2–5** are isostructural with **1**,[18] crystallising in the triclinic space group *P-1* (asymmetric unit contains {Dy$_3$} and half of M; see Figure S4 and Tables S1, S2). The coordination on Dy1 is disordered with MeOH/NO$_3$$^-$ modelled in the ratio 0.75:0.25. The Mn(O)$_6$ moiety in **2** has two short axial distances (1.919(2) Å) and four longer equatorial distances (av. 2.02 Å).

The chlorides **1'–5'** crystallise in the trigonal space group *R-3* (asymmetric unit contains one Dy, one sixth of M; see Figure S5 and Tables S3, S4). Each methanol is bound terminally to one Dy^{III} without disorder. Non-coordinating Cl$^-$ counter-anions lie above {Dy$_3$} triangles, directed towards H-atoms in μ$_3$-hydroxides (O–H···Cl = 3.179 Å) and coordinated methanols (O–H···Cl = 3.321 Å). The average Dy-ligand bond length is 2.382 Å. The average $M^{III}O_6$ bond lengths in **1'–5'** are 1.978, 1.990, 2.008, 1.908 and 1.893 Å, respectively. All six Mn–O distances in **2'** are equal by symmetry (1.99 Å). Other details are the same as for **1**.[18]
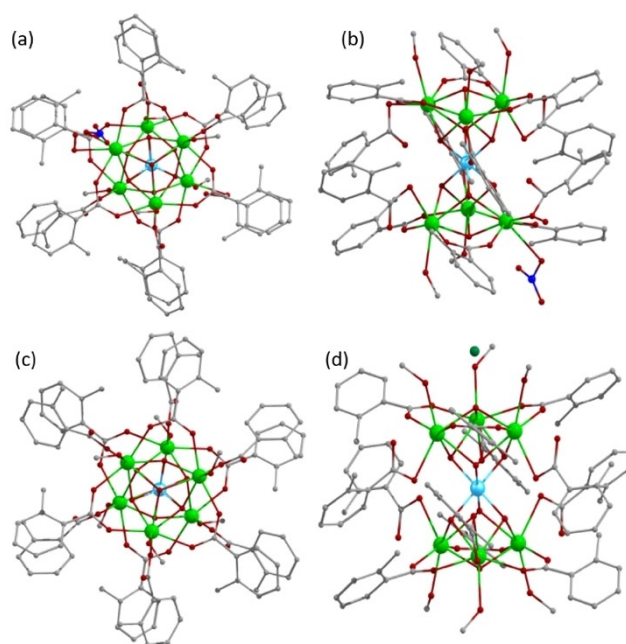

Figure 1. (a) Top and (b) side views of Mn-**2**, showing staggered {Dy$_3$} rings. Dy atoms green, Mn blue, O red, N blue. NB The disordered MeOH/NO$_3$ at Dy1 is shown as NO$_3$. (c) Top and (d) side views of Mn-**2'**; Cl in deep green.

Ab initio calculations

Using these atomic coordinates, we calculated *ab initio* at the CASSCF/RASSIO-SO level of theory the magnetic anisotropy, *g*-tensors and energy levels of each paramagnetic ion in **2–5** and **1'–6'** (details in SI). The axially-compressed Mn^{III} environment in **2** results in zero-field splitting (ZFS) with $D > 0$,[20] while the trigonally symmetric environments in **2'** and **6'** give $D < 0$.[21] Small values of D in **1'**, **3** and **3'** confirm expectations that Cr^{III} and Fe^{III} are near isotropic (see Table S5).

Similar to **1**,[18] inversion-related Dy^{III} ions possess effectively the same *g*-tensors, with very small transverse components (g_x, g_y) and large axial components (g_z) in the ground Kramers doublets (KDs, see Tables S6, S7) dominated by the microstates $m_J = \pm 15/2$ of the Dy^{III} $^6H_{15/2}$ ground level. Each Dy^{III} ion's magnetic easy axis almost lies in-plane and tangentially to a {Dy$_3$} triangle (Figure 2). Although the Dy^{III} axes form circular patterns, this alone does not prove the existence of toroidal ground states – for example, two Dy^{III} ions within a triangle may have their magnetic moments oriented clockwise, but the third Dy^{III} ion's moment may be oriented anticlockwise, producing a 'Dy-flipped' magnetic state. Rather, the ground states' identities also depend on the nature of the magnetic coupling between the Dy^{III} ions, and of course need to be consistent with analyses of the experimental data.

EurJIC
European Journal of Inorganic Chemistry

Full Papers
doi.org/10.1002/ejic.202001082

Chemistry
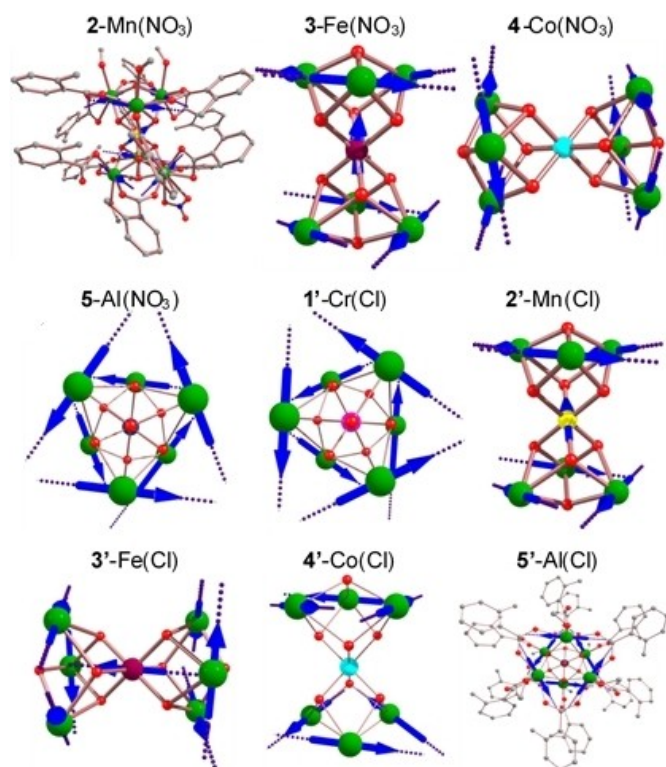**Europe**
European Chemical
Societies Publishing

Figure 2. Orientations of magnetic anisotropy axes (dotted lines) in each complex. For illustrative purposes, blue arrows depict the directions of local magnetic moments in one of the ground doublets, being FT for **1'/2/3'/4/4'/5/5'** (con-rotatory arrows), and AFT for **2'/3** (counter-rotatory arrows).
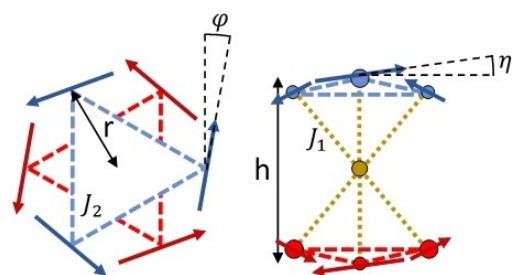

Figure 3. Top-view (left) and side-view (right) schematics of $\{Dy_3M^{III}Dy_3\}$, showing quantities in Table 1: h =centroid-to-centroid distance, r =average centroid-to-vertex distance, η =average out-of-plane angle of Dy easy axes (blue/red arrows), φ =average in-plane angle of axes from tangential directions, J_1 =M–Dy exchange coupling constant (dotted yellow lines), J_2 =intra-triangle Dy–Dy exchange coupling constant (dashed blue/red lines). (See SI for Hamiltonians and details of density functional theory (DFT) calculations for J_1 and J_2.)

Toroido-structural correlations: strategies to optimise ferrotoroidic coupling

Solely on the basis of the crystal structures and *ab initio* results, we have developed theoretical models (see SI) to calculate the exchange- and dipolar-coupled spectra of these complexes, and to analyse the correlations between their structures and SMT properties. Though the nitrate and chloride families had similar geometric proportions h and r (Figure 3), the M^{III} ionic radii (Figure S3) affected the ratios h/r listed in Table 1. As

expected,[18] this had important consequences for the ferrotoroidic coupling.

If the complexes had exact S_6 symmetry and Dy^{III} easy axes which were in-plane ($\eta = 0°$) and tangential to the triangles ($\varphi = 0°$), inter-triangle dipolar coupling would always produce FT ground states, with larger ΔE_{AFT-FT} for smaller h/r, as predicted in our previous work.[18] Crystal structures with pseudo-S_6 symmetry and $\eta, \varphi \neq 0$ as evaluated here (Table 1) can in principle disrupt this trend. For instance, as found in our previous work (see Supplementary note 3(i) in Ref. 18), AFT (FT) states are stabilised (destabilised) by out-of-plane components $\eta \neq 0$ of the magnetic states, on account of the reinforcing (cancelling) magnetic moments along the C_3 axis antiferromagnetically coupled to the central paramagnetic Cr ion in **1**.

Despite this, we find here that all predicted[18] trends are in fact verified within each series: smaller h/r (nitrates: $3 > 1 > 5 > 4$; chlorides: $3' > 1' > 5' > 4'$) causes larger ΔE_{AFT-FT} (nitrates: $3 < 1 < 5 < 4$; chlorides: $3' < 1' < 5' < 4'$). (NB This trend is overruled by Mn-anisotropy in **2/2'**.) Moreover, focusing on complexes with diamagnetic M and similar h/r to remove confounding factors, larger $|\eta|$ ($4' < 4 < 5 < 5'$) causes smaller ΔE_{AFT-FT} ($4' > 4 > 5 > 5'$).

Table 1. Effects of changing M and counter-anion on quantities in Figure 3, energy gaps between FT and AFT states (ΔE_{AFT-FT}), and energy gaps between FT states and lowest energy Dy-flipped magnetic state (ΔE_{Mag-FT}). NB The ground states are AFT in **3** and **2'**.

Complex	h [Å]	r [Å]	h/r	$\eta[°]$	$\varphi[°]$	$J_1[cm^{-1}]$	$J_2[cm^{-1}]$	ΔE_{AFT-FT} [cm^{-1}]	ΔE_{Mag-FT} [cm^{-1}]
1-Cr(NO$_3$)	5.385	2.176	2.475	6.635	0.930	−0.08	−0.043	0.159	3.041
2-Mn(NO$_3$)	5.429	2.177	2.494	−3.218	−2.235	+0.48	−0.053	0.210	2.491
3-Fe(NO$_3$)	5.444	2.176	2.502	−3.821	−1.305	+0.28	−0.01	−0.511	1.187
4—Co(NO$_3$)	5.274	2.170	2.431	−3.629	−0.620	N/A	−0.017	0.280	3.796
5-Al(NO$_3$)	5.308	2.174	2.442	4.576	0.871	N/A	−0.016	0.266	3.783
1'-Cr(Cl)	5.424	2.182	2.485	0.216	−2.295	−0.08[a]	−0.023	0.159	2.892
2'-Mn(Cl)	5.440	2.181	2.494	−3.657	0.499	+0.35	−0.01	−0.389	2.242
3'-Fe(Cl)	5.469	2.186	2.502	1.171	1.333	+0.31	−0.03	0.005	1.329
4'-Co(Cl)	5.301	2.173	2.440	−1.683	−0.018	N/A	−0.038	0.300	4.297
5'-Al(Cl)	5.345	2.186	2.445	−6.404	3.344	N/A	−0.033	0.188	3.988

[a] The value of J_1 for **1'**-Cr(Cl) was fitted from low-field, low-temperature powder magnetisation experimental data. See Figure S14 for more information.

EurJIC
European Journal of Inorganic Chemistry

Full Papers
doi.org/10.1002/ejic.202001082

Chemistry Europe
European Chemical
Societies Publishing

As predicted, the energetic effects of $\eta \neq 0$ increase when the AFT states' magnetic moments are stabilised by exchange/dipolar coupling with paramagnetic M ions, particularly for larger spins S_M and/or larger $|J_1|$. Comparing **3'** and **3** (equal h/r and S_M, similar J_1), the small $|\eta|$ in **3'** produces total Dy^{III} moments of $\mu(FT) = 0.011\,\mu_B$, $\mu(AFT) = 1.302\,\mu_B$ and FT ground states, whereas the larger $|\eta|$ in **3** gives $\mu(FT) = 0.078\,\mu_B$, $\mu(AFT) = 4.391\,\mu_B$ and *AFT ground states*.

Beside reporting here the discovery of a family of molecules bearing out all the predicted trends, we also uncover new trends. A paramagnetic M ion's ability to stabilise AFT states may be hindered by its anisotropy, if any. This is important in **2**, where easy-plane anisotropy prevents S_{Mn} from aligning with the AFT states' magnetic moments. Therefore, Mn^{III} only decreases ΔE_{AFT-FT} by $0.043\,cm^{-1}$, so the ground states remain FT in **2**. Conversely, the easy-axis anisotropy in **2'** allows Mn^{III} to couple with the AFT states' moments, decreasing ΔE_{AFT-FT} by $0.624\,cm^{-1}$, so the ground states are *AFT* in **2'**.

To summarise, although **2/3'** have the same M and h/r as **2'/3**, different $|\eta|$ and M-ion anisotropy produce FT ground states in **2/3'**, but AFT ground states in **2'/3**. We conclude that since it is difficult to experimentally control the anisotropies of seven ions simultaneously, the most practical strategy to produce large net toroidal moments in $\{Dy_3M^{III}Dy_3\}$ complexes is to use M ions which are small (for optimum h/r) *and* diamagnetic: ΔE_{AFT-FT} is consistently larger when M = Co, Al.

Signature of toroidal states on static magnetisation and dc susceptibility

Powder magnetisation isotherms (*M* vs. *H*) are shown in Figure 4. Interestingly, the saturation values (Table 2) all exceed the upper bounds predicted for randomly oriented powders (see SI). This means the crystallites have partially aligned with the external field, despite being dispersed in Vaseline. By contrast, our theoretical models' saturation magnetisations are all slightly below the upper bounds, as we assumed random crystallite orientations.

Although the AFT states in each complex are significantly populated at 2 K, their magnetic moments ($\sim 4\,\mu_B$) are much smaller than in the low-lying single-Dy-flipped states ($\sim 20\,\mu_B$) or double-Dy-flipped 'onion' states ($\sim 40\,\mu_B$). Therefore, the sizes of the energy gaps ΔE_{Mag-FT} determine whether *M* vs. *H* curves are S-shaped (large ΔE_{Mag-FT}), or rise sharply at low fields (small ΔE_{Mag-FT}).

For similar reasons to the ΔE_{AFT-FT} trends, ΔE_{Mag-FT} decreases as S_M, h/r, $|J_1|$, $|J_2|$, $|\eta|$ and/or $|\varphi|$ increase (nitrates ΔE_{Mag-FT}: $4 > 5 > 1 > 2 > 3$; chlorides ΔE_{Mag-FT}: $4' > 5' > 1' > 2' > 3'$, Table 1). Accordingly, the *M* vs. *H* curves for **2/2'/3/3'** all rise sharply at low fields, but the curves for **4/4'/5** are S-shaped (Figure 4). The curves for **1/1'** are also S-shaped despite moderate ΔE_{Mag-FT} values, because antiferromagnetic J_1 constants cause partial cancellations of Cr^{III} and Dy^{III} moments, rather than the addition of Mn^{III}/Fe^{III} and Dy^{III} moments seen in **2/2'/3/3'** with strongly ferromagnetic J_1.
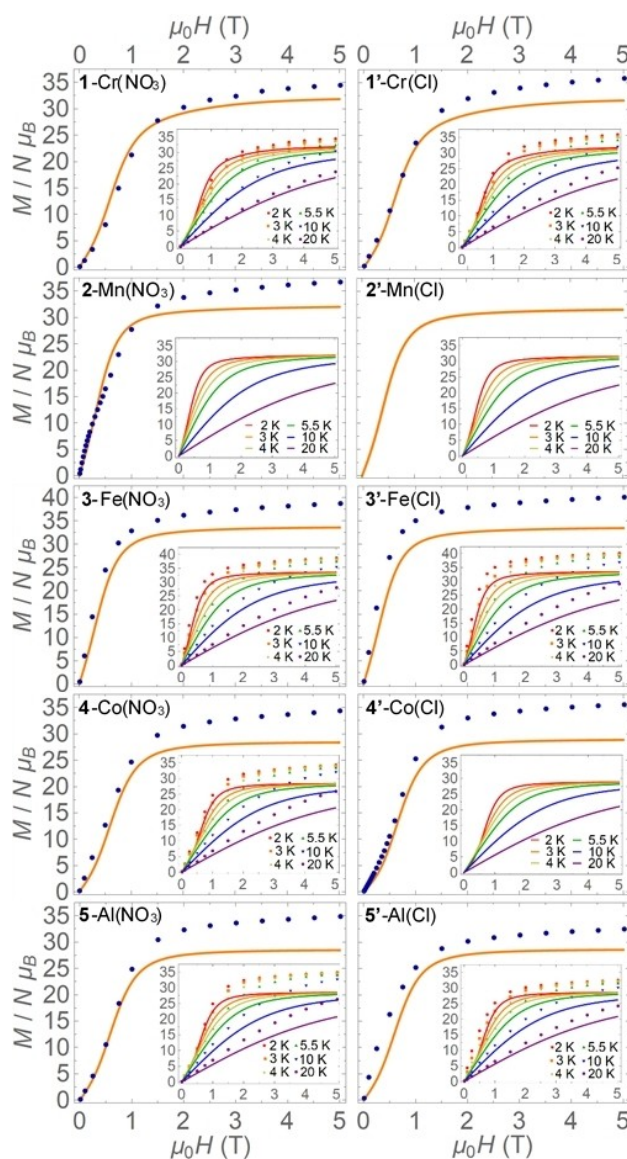

Figure 4. Plots of *M* vs. *H* data (dots) and parameter-free models (lines) at 2 K (main panels) and other temperatures (insets) for the nitrates (left) and chlorides (right). Experimental data for **1** are from Ref. 18.

Table 2. Saturation values for powder magnetisation and dc susceptibility. Except for $\chi_M T$ in **5'**, the experimental data always exceed the predicted upper bounds, which are slightly larger than the model values.

Complex	$M\,[N\mu_B]$ at 2 K, 5 T			$\chi_M T\,[cm^3\,K\,mol^{-1}]$ at 300 K, 1 T		
	Experiment	Bound	Model	Experiment	Bound	Model
1-Cr(NO₃)	34.47	32.25	31.82	87.16	86.91	85.99
2-Mn-(NO₃)	36.70	33.00	31.99	90.69	88.04	87.27
3-Fe(NO₃)	38.72	33.75	33.58	95.24	89.42	88.70
4-Co(NO₃)	34.38	30.00	28.37	86.06	85.03	84.15
5-Al(NO₃)	34.87	30.00	28.45	87.00	85.03	84.16
1'-Cr(Cl)	35.86	32.25	31.65	87.02	86.91	85.95
2'-Mn(Cl)	N/A	33.00	31.53	N/A	88.04	87.10
3'-Fe(Cl)	40.12	33.75	33.47	97.33	89.42	88.77
4'-Co(Cl)	35.54	30.00	28.84	89.44	85.03	84.01
5'-Al(Cl)	32.50	30.00	28.56	84.04	85.03	84.18

EurJIC
European Journal of Inorganic Chemistry

Full Papers
doi.org/10.1002/ejic.202001082

Chemistry Europe
European Chemical Societies Publishing

The only model that significantly disagrees with low-H experimental data is for **5′**, suggesting (i) overestimation of ΔE_{Mag-FT} due to inaccuracies in *ab initio* calculations for J_2, η and/or φ; or (ii) lasting alignment of **5′** crystallites with the external field after a previous experimental run to the data shown.

These findings highlight the need to develop parameter-free theoretical models independently of experimental measurements, where possible. If experiments and models disagree, the data should not be arbitrarily scaled to give agreement, as this obscures useful information. In this case, we learned that dispersing crystallites in Vaseline does not sufficiently suppress torqueing, so in future studies on similar complexes, we will use an alternative medium such as icosane, or press the powders in a nonmagnetic binder.

Independent theoretical analyses are particularly important in systems suspected to have toroidal moments. Experimental data alone may not be sufficient to identify the ground states as FT/AFT/magnetic, particularly when the associated energy gaps are small – the absence of an S-shaped M vs. H curve does not necessarily prove the absence of toroidal ground states.

Direct current (dc) magnetic susceptibility data are shown in Figure 5. The temperature variation of $\chi_M T$ is generally similar in all {Dy$_3$M^{III}Dy$_3$} complexes: it remains roughly constant between 300 and $\sim$100 K, then decreases gradually from thermal depopulation of Dy^{III} Stark levels, then drops rapidly below $\sim$10 K because the ground FT/AFT states have such small magnetic moments. (E.g. Dy-flipped magnetic states in **4** have net moments up to 39.681 μ_B, while $\mu(\text{FT}) = 0.012\ \mu_B$, $\mu(\text{AFT}) = 4.778\ \mu_B$.)

The $\chi_M T$ models (developed as per Ref. 18) accurately capture the low-T experimental behaviour, but often undershoot the mid-/high-T data, which is possibly related to inaccuracies in the *ab initio* excited KD energies (Table S6, Table S7). Alternatively, the discrepancy may indicate the crystallites have partially aligned with the field once again, despite being dispersed in Vaseline: while the modelled $\chi_M T$ products at 300 K, 1 T are slightly smaller than the high-T, non-interacting limits (Dy^{III}: $S = 5/2$, $J = 15/2$, $^6H_{15/2}$, $g = 4/3$, $C = 14.17$ cm^3 K mol^{-1}), the experimental data exceed these upper bounds for all complexes except **5′** (Table 2).

Unfortunately, we did not have enough bulk sample for magnetic studies on **2′**, but **6′** with diamagnetic Y^{III} has $\chi_M T \approx 3.0$ cm^3 mol^{-1} K between 300 and $\sim$20 K, and a rapid decrease below 20 K (Figure S10). This is consistent with the *ab initio* result of ZFS in high-spin d^4 Mn^{III}.

To explore the contributions of dipolar and exchange coupling, we also tested models with alternate values of J_1 and J_2 (Figures S7–S9, S11–S14). Though slight changes were observed, the main features of M vs. H and $\chi_M T$ vs. T experiments were reproduced even by 'dipolar-only' models. This means dipolar coupling, not exchange coupling, is the dominant intramolecular interaction in each {Dy$_3$M^{III}Dy$_3$} complex.
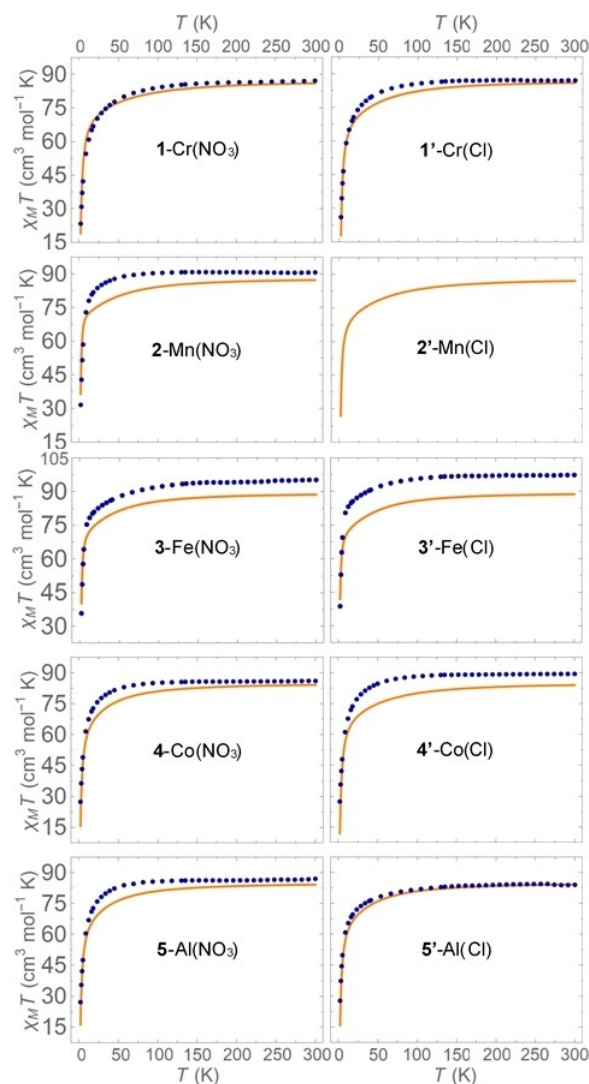

Figure 5. Plots of $\chi_M T$ vs. T data (dots) and parameter-free models (lines) at 1 T for the nitrates (left) and chlorides (right). Experimental data for **1** are from Ref. 18.

Ac susceptibility measurements

We measured alternating current (ac) magnetic susceptibilities at various temperatures, ac-frequencies and dc-field strengths (Figure S15). The out-of-phase components χ_M'' for complexes **1′/2/4/4′/5/5′** show larger ac-frequency dependence at smaller temperatures, indicating slow magnetic relaxation. This dependence became clearer for **4′** and **5′** in fixed dc-fields of $H_{DC} = 0.23$ and 0.2 T, respectively. However, in all cases, the maxima in χ_M'' are not well defined even at 2 K. This is especially apparent in **1′** and **5′** at $H_{DC} = 0.3$ T, where χ_M'' rises sharply with increasing ac-frequencies only below 2.6 K, similar to the behaviour observed in **1** for $H_{DC} = 0$, 0.2 T.[18] Complex **3** is an exception, with no clear ac-frequency dependence (indicating fast relaxation) when $H_{DC} = 0$ or 0.3 T. While the in-phase components χ_M' of **1′** and **5′** have broad, frequency-independ-

EurJIC
European Journal of Inorganic Chemistry

Full Papers
doi.org/10.1002/ejic.202001082

Chemistry Europe
European Chemical Societies Publishing

ent maxima at ~2.6 K when $H_{DC} = 0.3$ T, the maxima in χ_M' for **5** shift to higher temperatures with increasing ac-frequencies.

To better understand this behaviour, we performed single-ion *ab initio* calculations to produce qualitative mechanisms for Dy magnetic relaxation (Figure 6, Figure S16). Generally, the transition matrix elements for quantum tunnelling of the magnetisation (QTM) are small in ground KDs, e.g. 0.02 μ_B for Dy1 in **2** (Figure 6, top-left). (The Dy1 ion in **4** is an exception, with larger QTM (0.13 μ_B) allowing magnetic relaxation within its ground KD, which has a relatively larger ratio of $g_y/g_z = 0.0337$.) By comparison, the elements for thermally-assisted QTM (TA-QTM) are relatively large in first-excited KDs, e.g. 0.53 μ_B for Dy1 in **2**. Therefore, magnetic relaxation should mainly occur via first-excited KDs, and should be slowed by lower temperatures and larger energy barriers.

However, while TA-QTM may be a source of temperature-dependent magnetic relaxation, the first-excited KDs are too high in energy to fully explain the relaxation observed at such low temperatures as 2 K. Also, similar ac susceptibilities can be obtained from complexes with contrasting first-excited KD energies (different energies due to changes in M, e.g. ~120 cm^{-1} (**1'**) vs. ~90 cm^{-1} (**5'**), or coordination of -NO$_3$ vs. -Cl, as seen[22] in Dy^{III} single-ion magnets). This implies other relaxation mechanisms are taking place, such as Raman processes caused by spin-phonon coupling, intra-/intermolecular interactions, hyperfine couplings to nuclear spins in ^{161}Dy/^{163}Dy/ligands, etc.

Simulations of the hysteretic dynamics: crucial role of the M-linker in tuning toroidal-magnetic Zeeman level crossings

Single-crystal microSQUID measurements at various temperatures and field sweep rates are shown in Figures 7, S17–S22. All {Dy$_3$M^{III}Dy$_3$} complexes display magnetic hysteresis, though to varying extents, and a much larger dependence on temperatures than sweep rates. Comparing the nitrates (Figure 7, left) and chlorides (right), we observe relatively minor differences caused by subtle changes in geometric proportions (h, r), Dy^{III} easy axes (η, φ) and exchange coupling (J_1, J_2). Perhaps the most significant change between nitrate/chloride pairs is in **2**/**2'**, resulting from contrasting Mn^{III} anisotropies. However, we are mostly interested in how the physical mechanisms causing
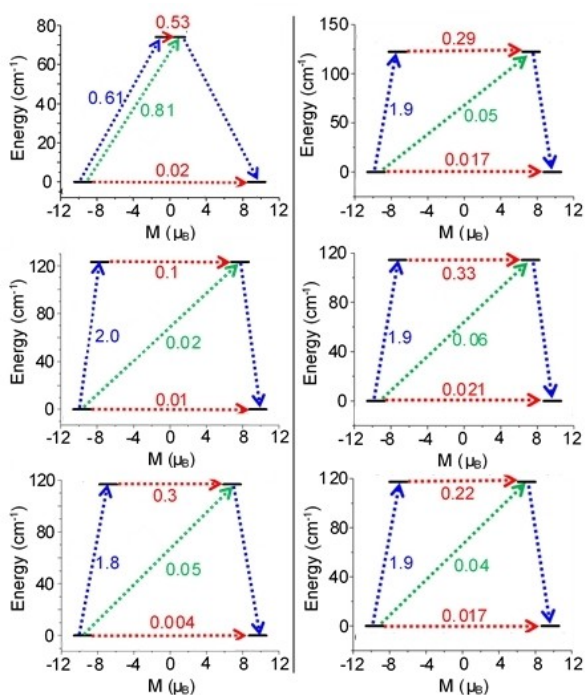

Figure 6. Qualitative mechanisms for magnetic relaxation of Dy1 (top), Dy2 (middle) and Dy3 (bottom) in **2** (left) and **1'** (right). The energies (vertical axis) and magnetic moments (horizontal axis) of ground/first-excited KDs (thick black lines) are shown. Numbers beside dotted arrows are the mean absolute values of transition matrix elements connecting the KDs via QTM (red arrows) or thermal excitations (blue/green arrows).
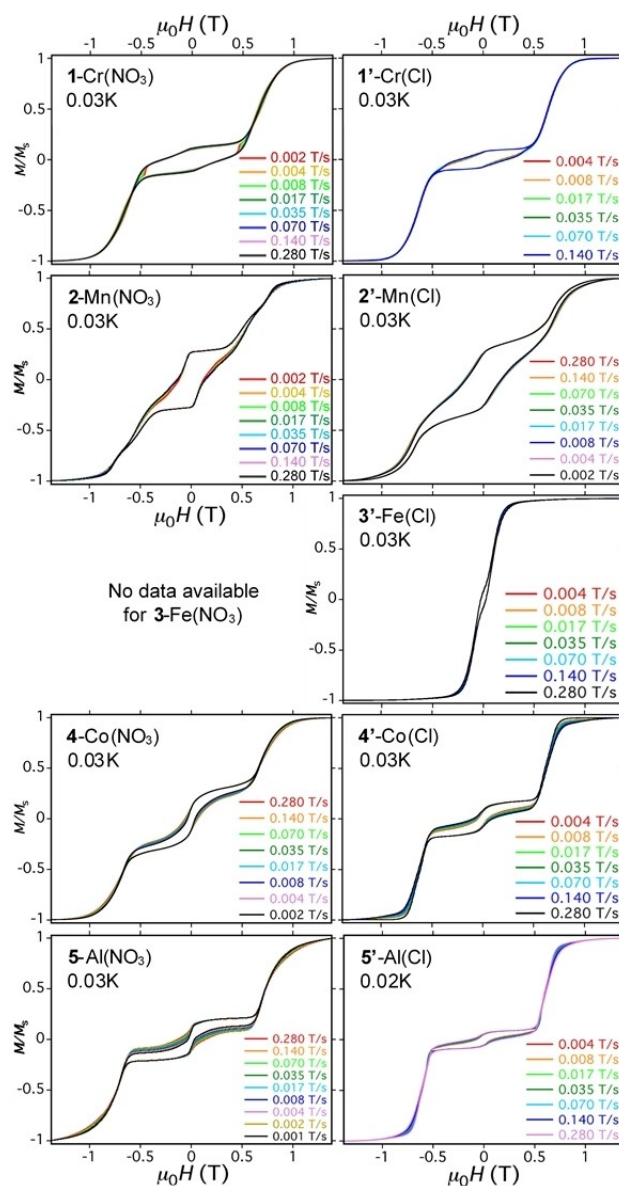

Figure 7. Single-crystal normalised magnetisation (M/M_S) vs. applied field for the nitrates (left) and chlorides (right), measured at the temperatures and scan rates indicated. Data for **1** are from Ref. 18.

EurJIC
European Journal of Inorganic Chemistry

Full Papers
doi.org/10.1002/ejic.202001082

Chemistry
Europe
European Chemical
Societies Publishing

hysteresis depend on M: diamagnetic vs. paramagnetic, isotropic vs. anisotropic.

To better understand the various hysteresis profiles observed, we extended the simulation program developed in Ref. 18 to account for changes in S_M, the field orientation, and the magnetic anisotropy of the central M^{III} ion. We also explored including two- and three-Dy-flip processes, inserting temperature- and field-dependence into the incoherent tunnelling prefactors γ_{ij}, and explicitly calculating the time-dependent broadening parameters λ_{ij} (see SI), but these extensions were ultimately removed from the simulations as they were not necessary to successfully reproduce the experimental behaviour.

By computationally exploring the parameter spaces for S_M, h, r, η, φ, J_1, J_2, various transition rates, and the applied field's orientation, we uncovered the following interesting trends:

- larger $|J_1|$, $|\eta|$ and/or $|\varphi|$ (to decrease ΔE_{Mag-FT}) gave smaller coercive fields H_C;
- more strongly antiferromagnetic J_2 (to increase ΔE_{Mag-FT}) gave larger H_C;
- changing the Cr^{III}-Dy^{III} exchange coupling to be ferromagnetic produced a larger remnant magnetisation M_{rem};
- larger $|\eta|$ and/or the field's out-of-plane angle η_F caused larger M_{rem} in **4/4'/5/5'**;
- increasing η_F and/or the field's in-plane angle φ_F 'stretched out' the hysteresis profiles (larger H_C, more gradual climbs in M/M_S at moderate fields);
- including more collective Dy^{III} states gave better agreement with the experimental temperature dependence (larger T reduces hysteresis, decreases M_S);
- larger single-Dy^{III}-flip tunnelling pre-factors $\gamma_{1Dy-flip}$ produced larger zero-field steps in M/M_S;
- larger single-Dy^{III}-flip spin-phonon pre-factors $\Gamma_{1Dy-flip}$ caused greater temperature dependence, smaller M_{rem} and steeper climbs in M/M_S at moderate fields;
- larger Dy^{III}-tunnelling broadening parameters $\lambda_{1Dy-flip}$ gave smoother hysteresis profiles;
- changing the M^{III} ion's transition rates had little effect on the simulated hysteresis, implying M-ion relaxation occurs on a much faster timescale than the field sweep rates.

Of course, when simulating experimental data (Figure 8, Figure 9), we fixed parameters as their calculated/measured values – the only free parameters were the field direction and single-Dy^{III}-flip transition rates. Nevertheless, by studying the trends above, we concluded that M^{III}-Dy^{III} dipolar/exchange coupling was stabilising collective Dy^{III} states to varying extents, and this was the main factor affecting the hysteresis. Indeed, the order of ground state level crossings in the Zeeman spectra (Figure 10) is of crucial importance, and is determined by the M ion's spin ($S_{Cr} = 3/2$, $S_{Mn} = 2$, $S_{Fe} = 5/2$, $S_{Co} = S_{Al} = 0$) and the value of J_1 (antiferromagnetic for M = Cr; ferromagnetic for M = Mn, Fe).

When a strong magnetic field acting on **1/1'/2/2'** is gradually decreased, the ground state's identity changes *directly* from an onion state (red lines in Figure 10) to either FT (green) or AFT (blue) states. Because these states are related to each other by multiple Dy^{III}-flips, there is little population transfer at
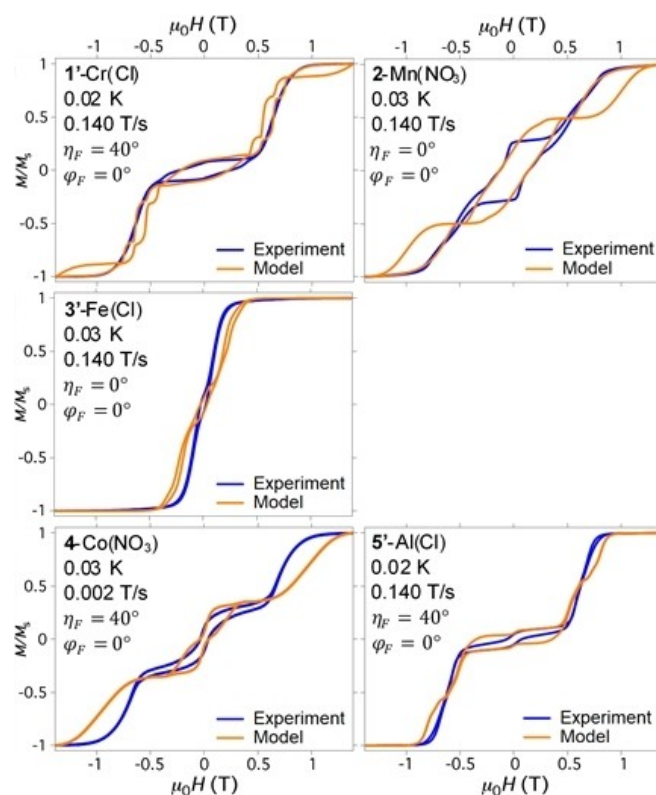

Figure 8. Measured and simulated hysteresis in complexes with different M ions. The field orientations and single-Dy-flip transition rates were determined by fitting experimental data (Table S8). NB Simulation for **4** used S_6-symmetric Dy axes with $\eta = 14°$, $\varphi = 0°$; see SI.
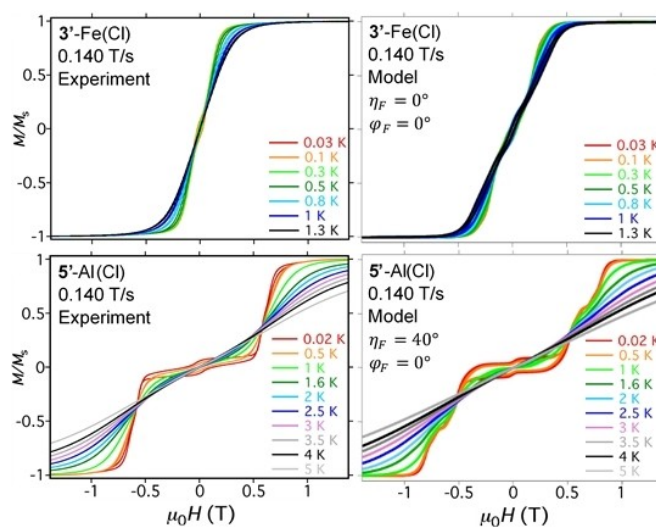

Figure 9. Variable-temperature hysteresis experiments (left) and models (right) for **3'** (top) and **5'** (bottom). As the temperature is increased, the preference is diminished for spin-phonon relaxation to populate the strongly magnetic onion states at high fields. Thus, saturation is either achieved at stronger fields than for lower temperatures (top), or not at all (bottom). To our knowledge, these are the first variable-temperature hysteresis simulations ever to be reported for lanthanide-based SMMs/SMTs.
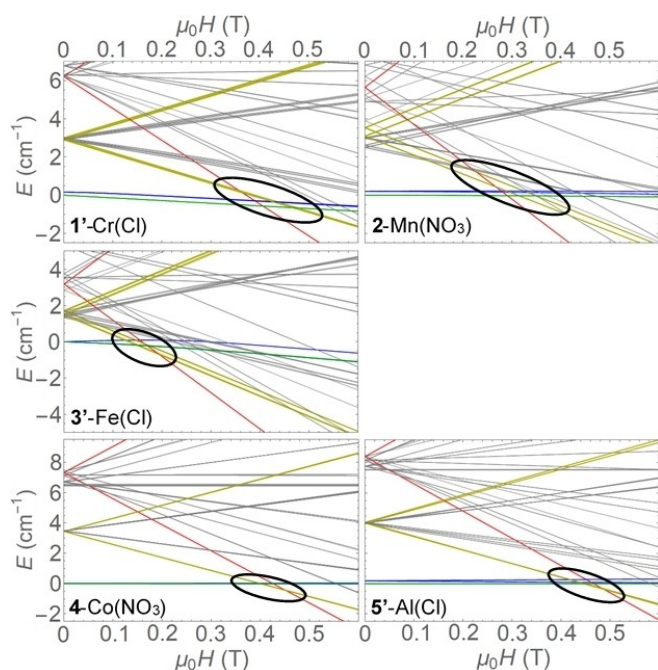
EurJIC
European Journal of Inorganic Chemistry

Full Papers
doi.org/10.1002/ejic.202001082

Chemistry
Europe
European Chemical
Societies Publishing

Figure 10. Zeeman spectra for various complexes (see also Figure S23); external fields oriented in-plane and tangential to {Dy$_3$} triangles ($\eta_F = \varphi_F = 0°$). Key level crossings are indicated by black ovals. For clarity, only ground M-eigenstates are shown for each collective Dy state. In order of increasing field-dependence, important Dy states are colour-coded: FT (green); AFT (blue); single-Dy-flipped (yellow); double-Dy-flipped (red). Unimportant Dy-flipped states (not aligned with field) are shown in grey. NB Spectrum for **4** used S_6-symmetric Dy axes with $\eta = 14°$, $\varphi = 0°$; see SI.
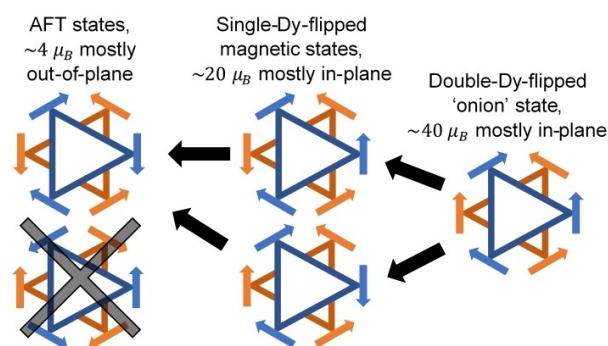

Figure 11. When a strong field is gradually decreased and the order of level crossings enables sequential one-flip transitions (black arrows), the AFT state which is two Dy-flips from the onion state becomes preferentially populated over the FT states (three Dy-flips from the onion state, not shown) and the other AFT state which is four Dy-flips from the onion state.

these initial level crossings. Rather, the double-Dy^{III}-flipped onion state's population partially tunnels into single-Dy^{III}-flipped states (yellow lines) at the next set of level crossings. While the field continues to decrease, spin-phonon relaxation transfers further population to the single-Dy^{III}-flipped states, then to the FT/AFT states. However, this occurs slowly at low temperatures, leaving the Dy^{III}-flipped states populated, so a non-zero M_{rem} is observed.

Depending on the M moment's direction relative to the net Dy^{III} moments, M may increase M_{rem} (ferromagnetic J_1 in **2/2'**) or decrease M_{rem} (antiferromagnetic J_1 in **1/1'**, though Cr^{III} does contribute to M_{rem} in FT states). As the field reverses, M/M_S declines because of tunnelling between various Dy^{III}-flipped states. Then, M/M_S becomes increasingly negative when the reversed field reaches level crossings between the FT/AFT states and single-Dy^{III}-flipped states. Some slight hysteresis occurs at high fields as spin-phonon relaxation gradually transfers population to the other onion state, and the cycle begins again.

Conversely, when a strong magnetic field acting on **4/4'/5/ 5'** is gradually decreased, the ground state's identity changes *sequentially*: onion to single-Dy^{III}-flipped to FT/AFT. This allows an efficient transfer of population into one of the AFT states (Figure 11), whose small out-of-plane moment produces a large portion of M_{rem}. Thus, differences between the hysteresis profiles of **4/4'/5/5'** arise from (i) changes in η affecting the AFT states' moments, (ii) varying ratios of AFT/Dy^{III}-flipped states'

contributions to M_{rem}, and (iii) different field orientations relative to the AFT states' moments.

Like in **1/1'/2/2'**, a step in M/M_S occurs at zero field as tunnelling events re-distribute the population remaining in the single-Dy^{III}-flipped states. However, this decline is brief and M/M_S plateaus after the field is reversed, because the AFT state's magnetisation cannot be depleted until tunnelling can eventually occur to the single-Dy^{III}-flipped states, then to an onion state.

Similar sequential level crossings are found in **3'** (Figure 10), but at smaller fields because M^{III}-Dy^{III} coupling stabilises the Dy^{III}-flipped states with respect to the FT/AFT states. Based on the sudden increase in the powder magnetisation for **3'** (Figure 4), and the very narrow hysteresis profile (Figure 7), we suspect our calculated value for J_1 is too small (or $|J_2|$ is too large), and the level crossings actually occur at even lower fields. This would explain the narrow hysteresis observed, with rapid changes in M/M_S arising from tightly spaced, sequential level crossings.

Hypothetically, without Mn^{III}-anisotropy in **2/2'**, the Mn^{III} moment would freely align with net Dy^{III} moments and stabilise Dy^{III}-flipped states even further, causing the key level crossings in **2** (**2'**) to occur at 0.10 T (0.17 T) rather than 0.28 T (0.25 T), respectively (Figure S24). As a result, the hysteresis profiles would be much narrower, possibly resembling that of **3'**. Therefore, Mn^{III}-anisotropy is a crucial factor in why **2/2'** display the broadest hysteresis profiles in the entire {Dy$_3$M^{III}Dy$_3$} series.

The diversity in the shapes of hysteresis profiles presented here highlights the need for detailed theoretical calculations to determine the nature of a molecule's ground state. Each new system must be analysed independently, without relying on similarities to hysteresis profiles of molecules previously found to be FT or AFT. For example, the complex **2'** possesses an AFT ground state, yet its hysteresis profile is very similar to that of a recently synthesised {Fe$_{18}$Dy$_6$} cyclic coordination cluster, whose ground state was predicted to be FT based on Dy–Dy spin-spin correlations.[23]

EurJIC
European Journal of Inorganic Chemistry

Full Papers
doi.org/10.1002/ejic.202001082

Chemistry
Europe
European Chemical
Societies Publishing

Conclusion

By thoroughly analysing an abundance of experimental data on ten derivatives of the parent double-triangle complex **1**-Cr(NO$_3$), we have discovered and confirmed several significant trends in their energetic, structural and magnetic properties. These trends are the first toroido-structural correlations ever to be reported and constitute a new type of magneto-structural correlations.

Particularly, we have shown that (i) small, diamagnetic M linking ions enhance the ferrotoroidic coupling between Dy$_3$ units; (ii) the ability of a paramagnetic M ion to stabilise antiferrotoroidic states may be hindered by its anisotropy, if any; (iii) by careful selection of the M ion, a complex's hysteresis profile can be tuned to increase the remnant magnetisation and/or coercive field.

By extending and generalising our hysteresis simulation program, we were able to analyse the slow magnetic relaxation for each choice of M ion and produce variable-temperature hysteresis simulations for these lanthanide-based SMMs/SMTs.

Future work could explore the possibility of removing the M ion altogether, and instead linking the triangles using covalent organic groups or π-π interactions in the ligands. This would likely lead to changes in the Dy^{III} ions' relative positions and easy axis orientations. However, if these challenges could be overcome while maintaining distinct toroidal moments on each triangle, the smaller range of h/r values accessible after removing the M ion would lead to even stronger ferrotoroidic coupling.

Our findings represent significant steps forward in understanding and optimising ferrotoroidal magnetism in lanthanide clusters. However, much more research still needs to be done into how we can incorporate these molecules into technological devices, and ultimately benefit from their fascinating magnetic properties.

Experimental Section

All experimental aspects of syntheses, structures, magnetism and theory are given in the SI.

Deposition Numbers 2003233 (for **2**), 2003234 (for **3**), 2003235 (for **4**), 2003236 (for **5**), 2003237 (for **1'**), 2003238 (for **2'**), 2003239 (for **3'**), 2003240 (for **4'**), 2004663 (**5'**) and 2004527 (for **6'**) contain the supplementary crystallographic data for this paper. These data are provided free of charge by the joint Cambridge Crystallographic Data Centre and Fachinformationszentrum Karlsruhe Access Structures service www.ccdc.cam.ac.uk/structures.

Acknowledgements

Conflict of Interest

The authors declare no conflict of interest.

[1] a) E. Coronado, A. J. Epstein, *J. Mater. Chem.* **2009**, *19*, 1670–1671; b) M. N. Leuenberger, D. Loss, *Nature* **2001**, *410*, 789–793.

[2] L. Bogani, W. Wernsdorfer, *Nat. Mater.* **2008**, *7*, 179–186.

[3] a) D. Gatteschi, R. Sessoli, J. Villain in *Molecular Nanomagnets*, Oxford University Press, Oxford, **2006**; b) D. Gatteschi, *Adv. Mater.* **1994**, *6*, 635–645.

[4] J. Luzon, K. Bernot, I. J. Hewitt, C. E. Anson, A. K. Powell, R. Sessoli, *Phys. Rev. Lett.* **2008**, *100*, 247205.

[5] a) A. Soncini, L. F. Chibotaru, *Phys. Rev. B* **2008**, *77*, 220406(R); b) L. F. Chibotaru, L. Ungur, A. Soncini, *Angew. Chem. Int. Ed.* **2008**, *47*, 4126–4129; *Angew. Chem.* **2008**, *120*, 4194–4197.

[6] L. Ungur, S.-Y. Lin, J. Tang, L. F. Chibotaru, *Chem. Soc. Rev.* **2014**, *43*, 6894–6905.

[7] A. Soncini, L. F. Chibotaru, *Phys. Rev. B* **2010**, *81*, 132403.

[8] a) D. I. Plokhov, A. K. Zvezdin, A. I. Popov, *Phys. Rev. B* **2011**, *83*, 184415; b) D. I. Plokhov, A. I. Popov, A. K. Zvezdin, *Phys. Rev. B* **2011**, *84*, 224436.

[9] a) J. M. Crabtree, A. Soncini, *Phys. Rev. B* **2018**, *98*, 094417; b) S. V. Rao, J. M. Ashtree, A. Soncini, *Physica B* **2020**, *592*, 412237.

[10] a) I. J. Hewitt, J. Tang, N. T. Madhu, C. E. Anson, Y. Lan, J. Luzon, M. Etienne, R. Sessoli, A. K. Powell, *Angew. Chem. Int. Ed.* **2010**, *49*, 6352–6356; *Angew. Chem.* **2010**, *122*, 6496–6500; b) S.-Y. Lin, W. Wernsdorfer, L. Ungur, A. K. Powell, Y.-N. Guo, J. Tang, L. Zhao, L. F. Chibotaru, H.-J. Zhang, *Angew. Chem. Int. Ed.* **2012**, *51*, 12767–12771; *Angew. Chem.* **2012**, *124*, 12939–12943; c) G. Novitchi, G. Pilet, L. Ungur, V. V. Moshchalkov, W. Wernsdorfer, L. F. Chibotaru, D. Luneau, A. K. Powell, *Chem. Sci.* **2012**, *3*, 1169–1176; d) L. Ungur, W. Van den Heuvel, L. F. Chibotaru, *New J. Chem.* **2009**, *33*, 1224–1230; e) M. Gysler, F. El Hallak, L. Ungur, R. Marx, M. Hakl, P. Neugebauer, Y. Rechkemmer, Y. Lan, I. Sheikin, M. Orlita, C. E. Anson, A. K. Powell, R. Sessoli, L. F. Chibotaru, J. van Slageren, *Chem. Sci.* **2016**, *7*, 4347–4354; f) D. Gatteschi, R. Sessoli, L. Sorace, *Chapter 286 - Magnetic Bistability in Lanthanide-Based Molecular Systems: The Role of Anisotropy and Exchange Interactions, in Handbook on the Physics and Chemistry of Rare Earths, Vol. 50* (Eds.: J.-C. Bunzli, V. Pecharsky), Elsevier, North Holland, **2016**, pp. 91–139; g) B. Hussain, D. Savard, T. J. Burchell, W. Wernsdorfer, M. Murugesu, *Chem. Commun.* **2009**, *0*, 1100–1102.

[11] a) C. Das, S. Vaidya, T. Gupta, J. M. Frost, M. Righi, E. K. Brechin, M. Affronte, G. Rajaraman, M. Shanmugam, *Chem. Eur. J.* **2015**, *21*, 15639–15650; b) P.-H. Guo, J.-L. Liu, Z.-M. Zhang, L. Ungur, L. F. Chibotaru, J.-D. Leng, F. S. Guo, M.-L. Tong, *Inorg. Chem.* **2012**, *51*, 1233–1235; c) A. I. Popov, D. I. Plokhov, A. K. Zvezdin, *Phys. Rev. B* **2016**, *94*, 184408.

[12] G. F. Garcia, D. Guettas, V. Montigaud, P. Larini, R. Sessoli, F. Totti, O. Cador, G. Pilet, B. Le Guennic, *Angew. Chem. Int. Ed.* **2018**, *57*, 17089–17093.

[13] a) L. Ungur, S. K. Langley, T. N. Hooper, B. Moubaraki, E. K. Brechin, K. S. Murray, L. F. Chibotaru, *J. Am. Chem. Soc.* **2012**, *134*, 18554–18557; b) A. Baniodeh, N. Magnani, S. Brase, C. E. Anson, A. K. Powell, *Dalton Trans.* **2015**, *44*, 6343–6347; c) S. K. Langley, K. R. Vignesh, B. Moubaraki, G. Rajaraman, K. S. Murray, *Chem. Eur. J.* **2019**, *25*, 4156–4165; d) S. K. Langley, K. R. Vignesh, T. Gupta, C. J. Gartshore, G. Rajaraman, C. M. Forsyth, K. S. Murray, *Dalton Trans.* **2019**, *48*, 15657–15667; e) L. Scherthan, T. Ruppert, Y. Peng, A. Baniodeh, H. Auerbach, T. Hochdörffer, J. A. Wolny, W. Bi, J. Zhao, M. Y. Hu, T. S. Toellner, E. E. Alp, D. E. Brown, C. E. Anson, A. K. Powell, V. Schünemann, *Hyperfine Interact.* **2019**, *240*, 124.

[14] a) H. Zhang, Y. Zhai, L. Qin, L. Ungur, H. Nojiri, Y. Zheng, *Matter* **2020**, *2*, 1–13; b) J. Wu, X.-L. Li, M. Guo, L. Zhao, Y.-Q. Zhang, J. Tang, *Chem. Commun.* **2018**, *54*, 1065–1068.

[15] Q. Zhang, M. L. Baker, S. Li, M. P. Sarachik, J. J. Baldoví, A. Gaita-Ariño, E. Coronado, D. I. Alexandropoulos, T. C. Stamatatos *Nanoscale* **2019**, *11*, 15131–15138.

[16] X.-L. Li, J. Tang, *Dalton Trans.* **2019**, *48*, 15358.

[17] S. Gnewuch, E. E. Rodriguez, *J. Solid State Chem.* **2019**, *271*, 175–190.

[18] K. R. Vignesh, A. Soncini, S. K. Langley, W. Wernsdorfer, K. S. Murray, G. Rajaraman, *Nat. Commun.* **2017**, *8*, 1023.

[19] K. R. Vignesh, S. K. Langley, A Swain, B. Moubaraki, M. Damjanović, W. Wernsdorfer, G. Rajaraman, K. S. Murray, *Angew. Chem. Int. Ed.* **2018**, *57*, 779–784; *Angew. Chem.* **2018**, *130*, 787–792.

[20] a) J. Krzystek, G. J. Yeagle, J.-H. Park, R. D. Britt, M. W. Meisel, L.-C. Brunel, J. Telser, *Inorg. Chem.* **2003**, *42*, 4610–4618; b) K. R. Vignesh, S. K. Langley, C. J. Gartshore, I. Borilović, C. M. Forsyth, G. Rajaraman, K. S. Murray, *Dalton Trans.* **2018**, *47*, 11820–11833.

[21] K. R. Vignesh, S. K. Langley, B. Moubaraki, K. S. Murray, G. Rajaraman, *Chem. Eur. J.* **2015**, *21*, 16364–16369.

[22] S. K. Langley, K. R. Vignesh, K. Holton, S. Benjamin, G. B. Hix, W. Phonsri, B. Moubaraki, K. S. Murray, G. Rajaraman, *Inorganics* **2018**, *6*, 61.

[23] H. Kaemmerer, A. Baniodeh, Y. Peng, E. Moreno-Pineda, M. Schulze, C. E. Anson, W. Wernsdorfer, J. Schnack, A. K. Powell, *J. Am. Chem. Soc.* **2020**, *142*, 14838–14842.